Title:

Heat advection processes leading to El Niño events as depicted by an ensemble of ocean assimilation products

Authors:

Joan Ballester (1,2), Simona Bordoni (1), Desislava Petrova (2), Xavier Rodó (2,3)

Affiliations:

(1) California Institute of Technology (Caltech), Pasadena, California, United States
(2) Institut Català de Ciències del Clima (IC3), Barcelona, Catalonia, Spain
(3) Institució Catalana de Recerca i Estudis Avançats (ICREA), Barcelona, Catalonia, Spain

Corresponding author:

Joan Ballester
California Institute of Technology (Caltech)
1200 E California Blvd, Pasadena, CA 91125, US
Mail Code: 131-24
Tel.: +1-626-395-8703
Email: joanballester@caltech.edu

Manuscript
Submitted to Journal of Climate

Abstract

The oscillatory nature of El Niño-Southern Oscillation results from an intricate superposition of near-equilibrium balances and out-of-phase disequilibrium processes between the ocean and the atmosphere. Several authors have shown that the heat content stored in the equatorial subsurface is key to provide memory to the system. Here we use an ensemble of ocean assimilation products to describe how heat advection is maintained in each dataset during the different stages of the oscillation.

Our analyses show that vertical advection due to surface horizontal convergence and downwelling motion is the only process contributing significantly to the initial subsurface warming in the western equatorial Pacific. This initial warming is found to be advected to the central Pacific by the equatorial undercurrent, which, together with the equatorward advection associated with anomalies in both the meridional temperature gradient and circulation at the level of the thermocline, explains the heat buildup in the central Pacific during the recharge phase. We also find that the recharge phase is characterized by increased meridional tilting of the thermocline and a southward upper-ocean cross-equatorial mass transport that results from Ekman-induced anomalous vertical motion in the off-equatorial regions.

The robust description of the role of heat advection emerging from the present work offers a reference for validation and assessment of climate model simulations through analysis of dynamical processes that are consistently represented in an ensemble of state-of-the-art ocean assimilation products, as well as those that are differently simulated by a subset of datasets, which ultimately determines an upper limit in the use of assimilation products for the validation of El Niño.

50

51 1. Introduction

52

53 El Niño-Southern Oscillation (ENSO) is the dominant source of interannual variability
54 worldwide and one of the most important modes of variability in the tropical Pacific, with far-
55 reaching influences on the whole climate system (Jin 1997a,b; Meinen and McPhaden 2000;
56 Wang 2002; Brown and Fedorov 2010; Ballester et al. 2011, 2013). The large amplitude of ENSO
57 anomalies in the tropical Pacific is essentially explained by the strong coupling between the
58 Walker circulation, the zonal gradient of sea surface temperature and the longitudinal tilt of the
59 thermocline (i.e. the so-called Bjerknes feedback; Bjerknes 1969; Wyrtki 1975). These interactions
60 are however modulated by out-of-phase negative feedbacks that bound the amplitude and
61 reverse the sign of interannual anomalies. According to the delayed oscillator theory, this
62 reversal is explained by the differential propagation speed of wind-induced oceanic Kelvin and
63 Rossby waves (Battisti 1988; Schopf and Suarez 1988). While eastward-propagating Kelvin
64 waves quickly deepen the warm ocean layer in the eastern Pacific (Wang 2002), westward
65 Rossby waves travel at lower speeds, and start to shallow the thermocline only after being
66 reflected as Kelvin waves at the western boundary (Fedorov and Brown 2009).

67 Among other models that have been proposed, the recharge oscillator emphasizes the
68 time delay between anomalies in longitudinally-averaged thermocline depth and eastern Pacific
69 sea surface temperature (Jin 1997a,b). In this conceptual framework, a deeper-than-normal
70 thermocline suppresses the active upwelling in the eastern Pacific and favors the growth of an
71 El Niño (EN) event and the weakening of the trade winds, whose curl generates poleward
72 Sverdrup transport that discharges the heat in the upper ocean and reverses the sign of ENSO
73 (Meinen and McPhaden 2000). This theory, therefore, hypothesizes that the oscillatory nature of
74 ENSO results from the balance between equatorial zonal winds and the pressure gradient

associated with the equatorial thermocline tilt, as well as from the disequilibrium between the mean basin-wide thermocline depth and the meridional convergence or divergence of Sverdrup transport due to tropical wind stress curl anomalies (Jin 1997a,b; Singh and Delcroix 2013).

Zonal and vertical currents are indeed intimately connected through the energy balance, because a significant fraction of the wind power is converted into buoyancy power (Brown and Fedorov 2010). This transfer explains how the energy supplied by enhanced trade winds to the westward South Equatorial Current (SEC) in the central Pacific is converted into downward (upward) mass fluxes in the western (eastern) Pacific that distort local ocean isopycnals and deepen (shoal) the thermocline (Brown et al. 2011). The increased (decreased) thermocline tilting in the equatorial Pacific associated with stronger (weaker) than normal trade winds induces large cold (warm) anomalies in sea surface temperature in the eastern Pacific, which are amplified by the ocean-atmosphere coupling and extended to the central Pacific by means of zonal advection.

The zonal advective, the Ekman pumping and the thermocline feedbacks have been described as the three major dynamical processes contributing to the amplification of temperature anomalies during the onset of ENSO events (Jin and Neelin 1993). Thus, assuming a small initial warm perturbation in the equatorial surface, the coupled system rapidly responds by weakening the trade winds and reducing the zonal tilting of the equatorial thermocline (Jin et al. 2006), which in turn generates anomalous eastward geostrophic currents in the central and eastern Pacific (Santoso et al. 2013). The upper ocean response is characterized by the decrease of the depth of the thermocline and the generation of anomalous zonal currents in the central and eastern Pacific, which together, amplify the initial anomalies and bring the oscillation to a mature phase (Jin and An 1999). These mechanisms also play an important role in the dampening and reversal of ENSO conditions when Sverdrup mass divergence starts to discharge the heat content in the equatorial Pacific after the mature phase of EN conditions.

100 The main objective of the present work is to perform an exhaustive spatiotemporal
101 analysis of the ocean heat advection mechanisms that characterize the stages of the ENSO
102 oscillation that lead to EN events. To this aim, we conduct our analyses to both highlight the
103 differences between the individual members of an ensemble of state-of-the-art ocean
104 assimilation products, and to put emphasis on those mechanisms that are common to all
105 datasets. The main results emerging from this study can hence be used as a reference for
106 validation and assessment of numerical simulations. While still largely disagreeing in some key
107 dynamical processes, given the large differences in their underlying models, assimilation
108 techniques and assimilated observations (Ray et al. 2015), these products provide the best and
109 most complete spatiotemporal picture of the ocean subsurface available to date. After
110 discussing our methodology (section 2), we use this ensemble of assimilation products to
111 describe the transitions that characterize the swing between phases of the oscillation, from a
112 climatological neutral base state (section 3) to the generation of a subsurface warm buildup in
113 the western Pacific (section 4), the recharged phase in basin-wide equatorial heat content
114 (section 5) and the onset and mature phases of EN (section 6). Discussion and summary are
115 provided in sections 7 and 8, respectively.
116
117
118 2. Methods
119
120 The onset of EN events is characterized by an initial subsurface heat buildup in the
121 western Pacific, the subsequent eastward movement of the accumulated warm waters along the
122 equatorial thermocline (i.e. recharge mode in the central Pacific) and the final rapid
123 amplification of temperature anomalies in the eastern Pacific due to the coupled ocean-
124 atmosphere Bjerknes feedback (Ballester et al. 2015). The present article describes the role of

heat advection in each of these three stages of the oscillation before the mature phase of EN events. To this aim, we analyze the different terms of the temperature tendency equation, which links the potential temperature (θ) tendency to the zonal (U_{adv}), meridional (V_{adv}) and vertical (W_{adv}) heat advection, thermal forcing (Q) and residual terms (R) through:

$$\frac{\partial \theta}{\partial t} = U_{adv} + V_{adv} + W_{adv} + Q + R \,. \quad (1)$$

We do not explicitly compute the thermal forcing as our focus is on the equatorial subsurface below the mixed layer, with climatological depths ranging from 20m in the eastern Pacific to 70m in the western Pacific (Zhang et al. 2007), where the effect of Q is small. The interannual anomalies of the heat advection components are expressed as

$$U_{adv}' = -\bar{u}\frac{\partial \theta'}{\partial x} - u'\frac{\partial \bar{\theta}}{\partial x} - u'\frac{\partial \theta'}{\partial x} + \overline{u'\frac{\partial \theta'}{\partial x}}\,, \quad (2)$$

$$V_{adv}' = -\bar{v}\frac{\partial \theta'}{\partial y} - v'\frac{\partial \bar{\theta}}{\partial y} - v'\frac{\partial \theta'}{\partial y} + \overline{v'\frac{\partial \theta'}{\partial y}} \text{ and} \quad (3)$$

$$W_{adv}' = -\bar{w}\frac{\partial \theta'}{\partial z} - w'\frac{\partial \bar{\theta}}{\partial z} - w'\frac{\partial \theta'}{\partial z} + \overline{w'\frac{\partial \theta'}{\partial z}}\,, \quad (4)$$

where the overbar and the prime denote the climatological and anomalous components, respectively, and u, v and w the zonal, meridional and vertical current velocities. Given that the contribution of the non-linear advection terms (i.e. the last two terms in equations 2-4) is generally small compared to the other components, they will not be explicitly described in this work, although they are implicitly included in the U_{adv}', V_{adv}' and W_{adv}' terms throughout this article.

Ocean potential temperature and zonal and meridional current velocities are obtained from 5 assimilation products: NEMOVAR-COMBINE (model: NEMO v3.0, Balmaseda et al. 2010), GECCO (MITgcm, Köhl and Stammer 2008), SODA2.2.6 (POP2.x, Carton and Giese 2008), ORAS4 (NEMO v3.0, Balmaseda et al. 2013) and ORAS3 (HOPE, Balmaseda et al. 2008). Vertical

147 velocity is diagnosed by integrating horizontal divergence down from the surface, with surface
148 values assumed to be equal to the time tendency of sea surface height. A 13-term running
149 average (1/24, 1/12, ..., 1/12, ..., 1/12, 1/24) is used to calculate the interannual anomaly
150 component of detrended monthly variables.

151 EN events are chosen according to the classification of the Climate Prediction Center:
152 December 1963, 1965, 1968, 1972, 1976, 1982, 1986, 1990, 1997, 2002, 2006 (CPC 2015). In those
153 cases when EN conditions are observed in the tropical Pacific for two consecutive boreal
154 winters (i.e. 1968/1969, 1976/1977, 1986/1987, 1990/1991), only the first year is considered for the
155 calculation of the composite anomalies, given that the main objective of the article is the
156 description of the onset of these events. The 1994 event was excluded from the analyses because
157 it was the continuation of a previous warm event starting in 1990, with warm sea surface
158 temperature anomalies persisting in the central and eastern tropical Pacific for almost 6 years
159 (Trenberth and Hoar 1996).

160

161

162 3. Climatological and ENSO year features

163

164 The main climatological features that characterize the circulation and the
165 thermodynamic structure of the equatorial and off-equatorial Pacific Ocean in the assimilation
166 products is consistent with previous observational studies and is shown in Figure 1. The
167 westward SEC is simulated in the tropical south Pacific, extending from 20S to about 3-4N
168 across the equator, where it is largely driven by the trade winds (Figures 1a,b). The circulation
169 in the equatorial Pacific is also characterized by the eastward Equatorial Under Current (EUC),
170 a subsurface current 200-400 km wide transporting 30-40 Sv along the tilted equatorial
171 thermocline (Izumo 2005, Figure 1b). The zonal velocity of the EUC is strongest in the central

172 Pacific at about 140W, and is primarily driven by the east-west pressure gradient in the
173 equatorial plane, in turn determined by the strength of the easterly zonal wind stress. In the
174 northern off-equatorial Pacific, the assimilation products also consistently reproduce the North
175 Equatorial Counter Current (NECC), whose eastward transport is determined by Sverdrup
176 dynamics and whose spatial structure is constrained by near-equatorial zonal wind stress (Yu et
177 al. 2000, Figure 1c).

178 The role of the trade winds is also key for explaining the spatial distribution of
179 temperature and vertical currents along the equatorial Pacific. The dynamical forcing associated
180 with the easterly wind stress piles up warm waters to the western Pacific and deepens the local
181 thermocline (Figures 1b,d). In this area, horizontal current convergence in the ocean surface
182 induces weak downwelling motion above the thermocline level, at the narrow westernmost
183 edge of the longitudinal band with strong easterlies (i.e. 150-160E, Ballester et al. 2015). In the
184 eastern Pacific, the wind stress forcing shoals the thermocline, with a zonal contrast of about
185 100-120 m in thermocline depth between the western and eastern parts of the basin (cf. Figures
186 1b,d,f). Ekman-driven equatorial upwelling in the central Pacific and coastal upwelling in the
187 eastern Pacific bring to the surface cold water from below the thermocline level, which explains
188 the equatorial minimum in surface temperatures relative to the off-equatorial bands (Figures
189 1e,f). The rising motion in the central Pacific is part of the shallow meridional overturning
190 circulation, with surface poleward divergence, symmetric downwelling motion in the off-
191 equatorial bands and meridional convergence at the pycnocline level (Izumo 2005; Figures 1a-
192 c,e).

193 The difference between the average thermodynamic structure in the equatorial and off-
194 equatorial Pacific Ocean during the mature phase of EN and La Niña (LN) events is shown in
195 Figure 2. During LN (EN) events, the strengthening (weakening or even reversal) of the trade
196 winds increases (decreases) the tilting of the thermocline and enhances (reduces) most features

of the oceanic circulation, including the SEC, the EUC, the downwelling motion in the western Pacific and the shallow meridional overturning cells in the central Pacific. Two prominent exceptions are found in the assimilation products. First, the eastward NECC is weakened (intensified) during the growing and mature phases of LN (EN) as a result of the decreased (increased) wind stress curl north of the equator (Hsin and Qiu 2012; Figure 2c), which together with the enhancement (suppression) of the westward SEC, contributes to the westward (eastward) displacement of the warm pool and the development of ENSO anomalies. Second, the equatorial upwelling in the far eastern Pacific is suppressed (intensified) during the peak of LN (EN) events (Figure 2f), being a primary out-of-phase reversal mechanism for the oscillatory nature of ENSO (Battisti 1988; Jin 1997a,b).

4. Growth of the warm buildup in the western and central Pacific (lags -33 to -21 before EN)

Figures 3-5 depict the multi-product average of the composite of EN events for the range of lags corresponding to the generation of the subsurface heat buildup in the western Pacific. The stippling highlights the inter-product similarities by showing the areas where anomalies are consistent among the datasets, approach that we take throughout the manuscript. The inter-product differences corresponding to the vertical, meridional and zonal advection terms are additionally presented in Figures 6,7, respectively. Here we show the longitude-depth values along a narrow band in the equatorial Pacific (2S-2N, Figures 3,6,7), and two latitude-depth meridional transects representative of the processes that lead to the initial stages of the heat buildup in the warm pool (150-160E, Figure 4) and to the east of the dateline (160-150W, Figure 5).

Ballester et al. (2015) highlighted fundamental differences between the dynamical origin of the subsurface warming in these two areas. On the one hand, in the western Pacific (130-170E), anomalous downwelling motion from an upper layer (0-75m) of horizontal convergence to a subsurface layer (75-190m) of horizontal divergence deepens the thermocline and advects heat downwards. Horizontal convergence near the surface is found to be an intricate combination of surface (0-60m) zonal convergence and subsurface (40-75m) meridional convergence, while the horizontal divergence just above the thermocline level is explained by the zonal component and the intensification of the EUC in the central Pacific. On the other hand, a completely different regime prevails in the central Pacific, where surface (0-60m) zonal and meridional divergence and subsurface (60-190m) zonal and meridional convergence generate strong upwelling motion.

The tendency equation reveals that a large fraction of the spatial structure of surface and subsurface heat anomalies in the equatorial Pacific is explained by zonal and vertical advective processes (cf. shading and contours in Figure 3b). To the west of 170E, vertical advection determines a large fraction of the subsurface warming (Figure 3h). In particular, this contribution is primarily explained by the vertical advection of the climatological temperature by anomalous currents ($-w'\partial\overline{\theta}/\partial z$, not shown), which results from the combination of (rather weak) downwelling anomalies (Figure 3a) and the strong climatological vertical gradient of temperature (Figure 1b). The decomposition of temperature anomalies along the meridional axis confirms the dominant role of vertical advection within the tropical band in this region (Figure 4). A tendency towards subsurface warming is present from 12S to 8N, which approximately corresponds to the latitudinal range with anomalous downwelling motion (Figure 4a). Nevertheless, the warming is clearly larger right at the equator near the thermocline, where both the vertical gradient of temperature and the anomaly in downward vertical velocity are largest (Figures 1d,4a). Figure 4 also confirms the negligible contribution of

247 zonal and meridional heat advection in this region at these very initial stages of the composite
248 of EN events, regardless of the specific latitudes within the tropical band.

249 To the east of 170E, the subsurface warming is a complex combination of different
250 mechanisms. The largest contribution to subsurface warming is associated with temperature
251 and circulation changes along the equatorial thermocline, which results from a combination of
252 the zonal and vertical terms (Figure 3b). In the case of the zonal component, the contribution of
253 the advection of anomalous heat by climatological currents (i.e. $-\overline{u}\partial\theta'/\partial x$) and the advection
254 of climatological temperature by anomalous currents ($-u'\partial\overline{\theta}/\partial x$) have similar magnitude,
255 with anomalies reaching up to +1 °C/year in the central Pacific near the thermocline level (not
256 shown). Note that nearly opposite anomalies are found for the vertical component (i.e.
257 $-\overline{w}\partial\theta'/\partial z$ and $-w'\partial\overline{\theta}/\partial z$).

258 The tendency in subsurface warming in the central Pacific is to a large extent explained
259 by $-(\overline{u}\partial/\partial x+\overline{w}\partial/\partial z)\theta'$ (cf. shading and contours in Figure 3c). This contribution is
260 associated with the negative eastward and upward gradient of subsurface temperature along
261 the equatorial thermocline due to increasing LN-like conditions (Figure 3a), which is advected
262 to the central Pacific by the climatological EUC (Figure 1b). These factors generate positive
263 zonal advection at the level of the thermocline and negative (positive) vertical advection above
264 (below) the thermocline (Figures 3f,h), which together explain the warming tendency observed
265 below 100-120m (Figure 3c). The overall contribution of $-(u'\partial/\partial x+w'\partial/\partial z)\overline{\theta}$ is instead
266 associated with the tilted stratification of the ocean (Figure 1b), which is advected by the
267 intensification of the EUC (Figure 3a). The diapycnal component of these circulation anomalies
268 is not negligible in this case, with eastward anomalies defining areas of warm advection at
269 160W and upward anomalies generating cold advection at 180 and 140W (Figure 3d).

In the central Pacific, the combination of the three components of heat advection essentially explains the tendency in subsurface temperatures (cf. shading and contours in Figure 5b). However, while the role of meridional advection is smaller than that of the zonal and vertical components, its contribution is important for describing the tendency of subsurface temperature in the off-equatorial bands (cf. Figures 5c,e). In fact, the zonal and vertical advection components tend to cancel each other in the latitude intervals 6-2S and 2-5N at 100m (Figures 5c,d,f), just above the thermocline (Figure 5a). The warming tendency in this area is instead entirely explained by the meridional advection of anomalous heat by climatological currents ($-\bar{v}\partial\theta'/\partial y$, not shown), which advects relatively less cold off-equatorial temperature anomalies (Figure 5a) through the equatorward lower branch of the climatological shallow meridional overturning cells (Figure 1e).

Although the above-described advection processes are generally reproduced by the five assimilation products, there are still substantial differences in their magnitude and spatial extent at this early stage of the oscillation. For example, all products reproduce the subsurface warming due to vertical advection to the west of 170E, but its intensity and extent varies greatly among the datasets: the downward advection is weak in ORAS3, confined to a narrow band in SODA2.2.6, close in magnitude to the composite average in NEMOVAR-COMBINE and ORAS4, and strong and extending eastwards to 160W in GECCO (Figure 6). These differences are essentially a reflection of differences in the ocean circulation, because of differing pattern and magnitude of the vertical velocity in each dataset (not shown). In turn, the warming due to zonal advection in the central Pacific is directly related to the subsurface warming tendency to the west of 170E, which is zonally advected along the thermocline by the EUC (not shown). Differences are even larger for the meridional component, with no contribution to the subsurface warming in GECCO, around average values in SODA2.2.6 and ORAS3, and a strong positive contribution in NEMOVAR-COMBINE and ORAS4 (Figure 7). The large differences in

295 the magnitude of the meridional term are seen to be key for explaining the different
296 propagation speed of the subsurface warming tendency along the thermocline (cf. contours in
297 Figure 7).
298
299
300 5. Transition to the recharged phase (lags -21 to -09 before EN)
301
302 The composites corresponding to the development of the basin-wide recharge mode in
303 equatorial heat content are shown in Figures 8 and 9. This phase is characterized by the peak in
304 LN-like conditions (Figure 8a) and a tendency towards warming of the equatorial Pacific
305 around the level of the thermocline (contours in Figure 8). In this section we show, as we did in
306 the previous section, the longitude-depth composite along the equatorial Pacific (2S-2N, Figure
307 8), as well as a latitude-depth meridional transect in the central Pacific (160-150W, Figure 9).
308 This transect corresponds to the area of maximum warming rate (i.e. largest temperature
309 tendency anomalies) and meridional mass exchange between the equatorial plane and the off-
310 equatorial bands. Despite some minor residual, the sum of the zonal, meridional and vertical
311 advection terms explains the general basin-wide subsurface warming near the thermocline (cf.
312 shading and contours in Figure 8b).
313 Similarly to what seen at earlier lags, in this stage of the ENSO cycle the most important
314 contribution to the subsurface warming in the equatorial central Pacific results once again from
315 both zonal and vertical terms of heat advection (Figure 8c). While the intensification of the EUC
316 is confined to 160-120W and is weaker than in the previous phase, heat advection anomalies are
317 largely explained by the strong eastward and upward gradient of anomalous temperature that
318 characterizes the peak of the LN-like conditions (Figure 8a). Further decomposition of these
319 terms reveals that $-(\overline{u}\partial/\partial x + \overline{w}\partial/\partial z)\theta'$ and $-(u'\partial/\partial x + w'\partial/\partial z)\overline{\theta}$ have opposite signs,

320 showing how temperature and circulation anomalies have opposing tendencies in the
321 subsurface temperatures in the central Pacific.

322 The mean advection of temperature anomalies $[-(\overline{u}\partial/\partial x + \overline{w}\partial/\partial z)\theta']$ is largely
323 positive in the whole central Pacific, from 170E to 120W and between 40 and 180m (Figure 8d).
324 This warm anomaly can be further decomposed in its zonal and vertical contributions, which
325 have large positive values at the level of the thermocline and at depths just above the
326 thermocline, respectively, as a result of the corresponding advection of the subsurface
327 anomalous heat buildup in the western Pacific (Figure 8a). The diapycnal transport is
328 characterized by the intensification of the Ekman-induced upwelling motion in the central
329 Pacific (Figure 8a), which drives cold waters to the surface and explains the negative anomalies
330 in $-w'\partial\overline{\theta}/\partial z$. The zonal component $-u'\partial\overline{\theta}/\partial x$ is positive at the level of the thermocline,
331 due to the weak intensification of the zonal component of the EUC (Figures 8a,f). Nevertheless,
332 anomalies in the vertical component dominate, controlling the overall sign of
333 $-(u'\partial/\partial x + w'\partial/\partial z)\overline{\theta}$ (Figure 8e).

334 While playing a relatively minor role in the central Pacific (cf. Figures 8c,g), meridional
335 heat advection along the equatorial thermocline explains a large fraction of the subsurface
336 warming in the eastern Pacific. Advection of mean temperatures by anomalous currents,
337 $-v'\partial\overline{\theta}/\partial y$, and of anomalous temperatures by mean currents, $-\overline{v}\partial\theta'/\partial y$, both contribute to
338 the overall meridional advection pattern. As shown in Figure 9a, in the central Pacific
339 anomalous currents are characterized by a strengthening of the shallow meridional overturning
340 cells, with anomalous surface Ekman divergence, off-equatorial downwelling and subsurface
341 convergence. Thus, the subsurface convergence in meridional currents advects climatological
342 off-equatorial warmer waters to the equator (Figure 1e). Similarly, temperature anomalies show
343 weak warming in the off-equatorial regions near the level of the thermocline (Figure 9a), which

are advected to the equator by the climatological shallow meridional overturning circulation (Figure 1e). When considering the near-equatorial band as a whole (e.g. 10S-10N), it is clear from the latitudinal transect that the combined contribution of the zonal (Figure 9c) and vertical (Figure 9e) components dominate over the meridional term in determining the subsurface warming in the recharge mode (cf. Figures 9b,d). Results also show that half of the contribution of the meridional advection is explained by the intensification of the ocean circulation, and the other half by the deepening of the off-equatorial thermocline (Figures 8i,8j,9a).

The inter-product comparison reveals that very large differences exist between ensemble members at this intermediate phase of the oscillation. For example, the sum of the zonal and vertical advection terms contributes differently to the temperature tendency in each dataset: This contribution is only positive in 170E-150W at 100-200m depth in NEMOVAR-COMBINE and ORAS4, weakly positive in 160E-140W at around 100m in SODA2.2.6, and positive in the whole equatorial Pacific at 20-140m in ORAS3 and at 80-160m in GECCO (Figure 10). These differences primarily arise from the vertical component, given that the diapycnal upwelling of cold subsurface waters across the thermocline is subject to large uncertainties (not shown). Instead, the meridional term only differs in magnitude and not in sign or spatial extent (Figure 11). Interestingly, the larger the contribution of the meridional advection to the subsurface warming, the larger the warming tendency near the thermocline level (cf. shading and contours in Figure 11), regardless of the contribution of the zonal and vertical components (Figure 10), indicating the dynamical importance of the meridional term at this phase.

6. Onset of EN events (lags -09 to +00 before EN)

368 Figures 12 and 13 depict composites corresponding to the onset and growing phase of
369 EN events. The oceanic conditions during this phase are characterized by warm subsurface
370 anomalies along the equatorial thermocline and the weakening (enhancement) of the EUC in
371 the western (eastern) Pacific (Figure 12a). The SEC, the downwelling motion in the warm pool
372 and the coastal upwelling in the far eastern Pacific are also found to be weaker than in the
373 climatology (Figure 12a). These anomalies are known to be associated with the tendency
374 towards warm EN conditions in the central and eastern Pacific, including the beginning stage of
375 weakened trade winds, the flattening of the equatorial thermocline and the development of a
376 subsurface cold buildup in the western Pacific (contours in Figure 12). The role of advective
377 processes is here briefly revisited through the longitude-depth composite along the equatorial
378 Pacific (2S-2N, Figure 12) and the latitude-depth meridional transect in the central Pacific (160-
379 150W, Figure 13).

380 Similarly to the previous phases, the combination of the three advection terms is in
381 good agreement with the magnitude and spatial structure of the tendency in subsurface
382 temperature (cf. shading and contours in Figure 12e). Note that this correspondence is again
383 primarily explained by the combined contribution of the zonal and vertical advection (Figure
384 12b). On the one hand, the advection of climatological temperature by anomalous zonal
385 currents (i.e. $-u'\partial\overline{\theta}/\partial x$) is well known to be largely responsible for the warming tendency in
386 the central and eastern upper ocean (zonal advection feedback, An and Jin 2001, see Figure 12f
387 as a reference). On the other hand, the advection of climatological heat by anomalous vertical
388 currents ($-w'\partial\overline{\theta}/\partial z$) has been described as a fundamental process for the warming in the far
389 eastern Pacific (Ekman pumping feedback, Jin et al. 2006, Figure 12h).

390 The meridional transect in the central Pacific shows that the largest heat anomalies are
391 confined to the latitudinal range 5S-5N, between 100m and the thermocline level (Figure 13a).
392 The vertical velocity anomalies are characterized by strong upwelling north of the equator (6N-

9N) and strong downwelling south of it (4S-1S) (Figure 13a). Thus, anomalies in the northern hemisphere tend to restore the thermocline to its climatological depth, while those in the southern hemisphere contribute to the deepening of the thermocline near the equator by intensifying the northernmost edge of the downwelling branch of the southern shallow meridional overturning cell (Figure 1e). Interestingly, inter-hemispheric differences in vertical velocity anomalies increase the meridional tilting of the thermocline and generate southward cross-equatorial mass transport in the upper 50m of the ocean (Figure 13a).

The meridional heat advection is negative in the central and eastern Pacific near the level of the thermocline (Figure 12g). As a result, this component starts contributing to the weakening of the heat content in the equatorial Pacific subsurface already in the recharge phase (Figure 12a), before the onset of EN and the activation of the Bjerknes feedback. The decomposition of this term shows that $-\bar{v}\partial\theta'/\partial y$ is larger and has opposite sign relative to $-v'\partial\bar{\theta}/\partial y$ (cf. Figures 12c,d). Indeed, $-\bar{v}\partial\theta'/\partial y$ ($-v'\partial\bar{\theta}/\partial y$) shows large negative (weak positive) anomalies in the off-equatorial regions (Figures 13c,d), near the areas of climatological (anomalous) subsurface equatorward convergence and strong meridional contrast in anomalous (climatological) temperature (Figures 1e,13a).

7. Discussion: integrated depiction of the ENSO cycle

Figure 14 provides an integrated view of the ENSO oscillation by showing the contribution of the processes described throughout the manuscript to the equatorial temperature tendency at the thermocline level and as a function of the time lag. This comparison highlights the generally synchronous evolution of the temperature tendency and the advection along the tilted equatorial thermocline (cf. shading and contours in Figure 14c). In

418 the central Pacific (170E-110W), this tendency is to a large extent explained by the advection of
419 the initial subsurface warm buildup in the western Pacific by the climatological EUC (i.e.
420 $-(\overline{u}\partial/\partial x + \overline{w}\partial/\partial z)\theta'$, Figure 14d). Instead, the anomalous downwelling motion of surface
421 climatological warm waters ($-w'\partial\overline{\theta}/\partial z$) is the key process explaining the evolution of the
422 subsurface warming in the western (130-170E) and far eastern (110-90W) Pacific (Figure 14e).
423 Note that the transition between advective processes near 170E is explained by a clear regime
424 shift in the vertical structure of horizontal divergence (Ballester et al. 2015).

425 The latitudinal heat advection structure is illustrated in the south-north transect in the
426 central Pacific shown in Figure 15. The contribution of the meridional term is negligible right at
427 the equator, where the Ekman-induced upwelling motion dominates, but it rapidly increases
428 polewards, attaining anomalies that are already large at 2S and 2N (Figure 15g). Here we
429 considered a narrow equatorial band (i.e. 2S-2N) in order to isolate the ascending branch of the
430 shallow meridional overturning cells from the descending branches at around 8-3S and 3-8N
431 (Figure 1e). Note that this circulation is associated with a cross-shaped anomalous pattern in
432 both the zonal and vertical advection terms (Figures 15f,h), which is not found in their
433 combined contribution (Figure 15c). The meridional advection remains qualitatively
434 unmodified when the latitudinal range considered for the equatorial averages in the longitude-
435 depth plane includes the descending branches of the cells (e.g. 6S-6N, not shown).

436 The peak in LN (EN) conditions is approximately in phase with the equatorward
437 meridional warm (cold) advection in the central and eastern Pacific (Figure 14g). The phase of
438 the oscillation in which the contribution of meridional advection reaches its peak is however the
439 result of the combination of two different processes with different temporal evolution. On the
440 one hand, the discharge (recharge) phase in basin-wide equatorial heat content leads to LN
441 (EN) events by approximately 9 months (Meinen and McPhaden 2000). This phase is
442 characterized by colder (warmer) temperature anomalies at the equator than in the off-

443 equatorial regions (e.g. Figure 13a). Thus, the meridional circulation of the climatological
444 shallow meridional overturning cells warms (cools) the equatorial and off-equatorial
445 thermocline before the mature phase of LN (EN) events ($-\bar{v}\partial\theta'/\partial y$; Figures 14i,15i). On the
446 other hand, the strengthening (weakening) of the equatorial trade winds during LN (EN)
447 conditions, as well as the associated changes in off-equatorial wind stress curl, induces
448 anomalous subsurface equatorward (poleward) Sverdrup transport of mass (Jin 1997a,b). The
449 disequilibrium balance between these processes generates a delayed warming (cooling) at the
450 level of the thermocline ($-v'\partial\bar{\theta}/\partial y$; Figures 14j,15j).

451 In this regard, the synchronous evolution of LN (EN) conditions and the equatorward
452 warm (cold) advection in the central and eastern Pacific, as illustrated in Figure 14g, is shown to
453 be compatible with the recharge theory formulated by Jin, which is mathematically described
454 by the tilting mode and the recharge-discharge phase. The tilting mode characterizes the quick
455 oceanic response to enhanced (weakened) easterly wind stress in the central tropical Pacific
456 during LN (EN) conditions, which is proportional to the zonal tilting of the equatorial
457 thermocline. The recharge (discharge) phase provides the required memory between opposite
458 phases of the tilting mode. This transition period is characterized by the time tendency towards
459 anomalous equatorward (poleward) Sverdrup convergence (divergence) of mass due to
460 enhanced (weakened) easterly wind stress in the western and central tropical Pacific, and its
461 associated change in the off-equatorial curl, which ultimately tends to deepen the thermocline.

462 The recharge theory is also found to be compatible with the longitudinal transition in
463 the mechanisms explaining the initial subsurface heat buildup on either side of 170E, as well as
464 the subsequent eastward propagation along the equatorial thermocline. Near and east of the
465 dateline, anomalous easterly (westerly) trade winds during LN (EN) events are associated with
466 the tendency towards equatorward (poleward) Sverdrup mass convergence (divergence) and
467 the deepening of the thermocline (e.g. Figure 8j). Near the edge of the warm pool, easterly

(westerly) wind stress anomalies and the associated anticyclonic (cyclonic) curl anomalies are weaker, and therefore this delayed effect is smaller (Figure 8j). The oceanic response in this region appears to be more directly controlled by the zonal convergence (divergence) of the zonal wind stress along the equator, which favors anomalous surface ocean horizontal convergence (divergence) and downward (upward) motion during LN (EN) events (Ballester et al. 2015; Figures 3h,4e). This process explains the much faster, albeit still somewhat delayed, response of subsurface temperatures in the warm pool (e.g. the zero contour in Figure 14e crosses longitude 160E at lag +03). The present article clarifies, within the context of the recharge oscillator theory, the relative contribution, spatial extent and delayed effect of each of the mechanisms involved in the subsurface buildup in the western and central Pacific, and its eastward propagation.

8. Summary and conclusions

The present work describes different processes that control subsurface temperatures and thermocline depth during the generation of El Niño events through a careful analysis of the subsurface heat budget. All terms in this analysis are inferred from an ensemble of state-of-the-art ocean assimilation products, focusing on those processes that are robustly produced by all the members of the ensemble, as well as those that are differently simulated by a subset of datasets. The combined use of multiple ocean analysis products provides an unprecedented three-dimensional description of mechanisms leading to the generation of EN events. Additionally, it allows for a more detailed validation and assessment of mechanisms previously inferred from intermediate and complex coupled climate models, as well as for the determination of the limits in the use of assimilation products for the validation itself.

493 We emphasize the role that different processes play in the evolution of subsurface
494 warm anomalies during the different stages of the oscillation. Main results include:
495 • To the west of 170E, the vertical advection of climatological temperature by
496 anomalous currents, induced by surface horizontal convergence, downwelling
497 motion and subsurface divergence, was shown to explain alone the initial
498 subsurface warming in the equatorial and off-equatorial Pacific during the warm
499 buildup stage, between monthly lags -33 to -21 before the peak of EN events.
500 • The role of horizontal advection was found to be confined to the east of 170E,
501 explaining the tendency towards the return to climatological conditions of
502 subsurface temperatures in the central Pacific, both through zonal and vertical
503 advection along the equatorial thermocline and through meridional advection
504 right above this level.
505 • These two mechanisms were also shown to explain a large fraction of the subsurface
506 warming associated with the recharge phase in basin-wide heat content. On the
507 one hand, along the meridional axis, the equatorward advection of heat was shown
508 to be explained to the same extent by anomalies in the meridional gradient of
509 subsurface temperature and anomalies in the meridional ocean circulation. On the
510 other hand, along the equatorial plane (i.e. combination of the zonal and vertical
511 components), the anomalous heat accumulated in the western Pacific was seen to
512 be advected to the central Pacific by the climatological currents. This contribution
513 was found to be partially counterbalanced by the advection of climatological
514 temperature by the anomalous currents, which is dominated by anomalous
515 diapycnal upwelling of cold subsurface waters.
516 Mechanisms described in the present work can be used as a reference for the validation
517 of numerical simulations from intermediate and complex coupled climate models. For example,

518 a key feature highlighted here is the asymmetry between the northern and the southern tropical
519 hemispheres during the recharge mode. This phase is characterized by an increase of the
520 meridional tilting of the thermocline and the southward cross-equatorial mass transport in the
521 upper ocean as a result of the anomalous upwelling (downwelling) motion in 6-8N (3-1S). Yu
522 and Mechoso (2001) showed that the anomalies in vertical velocity are due to the latitudinal
523 distribution of zonal wind stress anomalies, which induces areas of convergence and
524 divergence of meridional Ekman transport. Nonetheless, the climate model used by Yu and
525 Mechoso (2001) simulated vertical anomalies of equal sign and no cross-equatorial anomalies
526 between the off-equatorial regions, in disagreement with our results. This highlights how the
527 present work provides an unprecedented description of the dynamical processes that might
528 prove useful to the climate modeling community to test the performance of the ENSO
529 oscillation in state-of-the-art climate models.
530
531
532 Acknowledgements
533
534 JB gratefully acknowledges funding from the European Commission through a Marie
535 Curie International Outgoing Fellowship of the 7th Framework Programme for Research
536 (project MEMENTO from the FP7-PEOPLE-2011-IOF call). X.R. acknowledges funding from the
537 EUFP7 projects DENFREE and EUPORIAS.
538
539
540 References
541

An SI, Jin FF. Collective Role of Thermocline and Zonal Advective Feedbacks in the ENSO Mode. Journal of Climate 14, 3421-3432 (2001).

Ballester J, Bordoni S, Petrova D, Rodó X. On the dynamical mechanisms explaining the western Pacific subsurface temperature buildup leading to ENSO events. Geophysical Research Letters, doi:10.1002/2015GL063701 (2015).

Ballester J, Rodríguez-Arias MA, Rodó X. A new extratropical tracer describing the role of the western Pacific in the onset of El Niño: Implications for ENSO understanding and forecasting. Journal of Climate 24, 1425-1437 (2011).

Ballester J, Burns JC, Cayan D, Nakamura Y, Uehara R, Rodó X. Kawasaki disease and ENSO-driven wind circulation. Geophysical Research Letters 40, 2284-2289 (2013).

Balmaseda MA, Mogensen K, Molteni F, Weaver AT. The NEMOVAR-COMBINE ocean re-analysis. COMBINE Technical Report No. 1, (2010).

Balmaseda MA, Mogensen K, Weaver AT. Evaluation of the ECMWF ocean reanalysis system ORAS4. Quarterly Journal of the Royal Meteorological Society 139, 1132-1161 (2013).

Balmaseda MA, Vidard A, Anderson DLT. The ECMWF Ocean Analysis System: ORA-S3. Monthly Weather Review 136, 3018-3034 (2008).

Battisti DS. Dynamics and Thermodynamics of a Warming Event in a Coupled Tropical Atmosphere-Ocean Model. Journal of the Atmospheric Sciences 45, 2889-2919 (1988).

Bjerknes J. Atmospheric teleconnections from the equatorial Pacific. Monthly Weather Review 97, 163-172 (1969).

Brown JN, Fedorov AV, Guilyardi E. How well do coupled models replicate ocean energetics relevant to ENSO? Climate Dynamics 36, 2147-2158 (2011).

Brown JN, Fedorov AV. How Much Energy Is Transferred from the Winds to the Thermocline on ENSO Time Scales? Journal of Climate 23, 1563-1580 (2010).

566 Carton JA, Giese BS. A Reanalysis of Ocean Climate Using Simple Ocean Data
567 Assimilation (SODA). Monthly Weather Review 136, 2999-3017 (2008).
568 CPC. Cold and Warm Episodes by Season.
569 http://www.cpc.ncep.noaa.gov/products/analysis_monitoring/ensostuff/ensoyears.shtml. Last
570 accessed in January 2015 (2015).
571 Fedorov AV, Brown J. Equatorial waves. Encyclopedia of Ocean Sciences, 2nd ed, Ed J
572 Steele, Academic Press, 3679-3695 (2009).
573 Hsin YC, Qiu B. The impact of Eastern-Pacific versus Central-Pacific El Niños on the
574 North Equatorial Countercurrent in the Pacific Ocean. Journal of Geophysical Research 117,
575 C11017 (2012).
576 Izumo T. The equatorial undercurrent, meridional overturning circulation, and their
577 roles in mass and heat exchanges during El Niño events in the tropical Pacific ocean. Ocean
578 Dynamics 55, 110-123 (2005).
579 Jin FF. An Equatorial Ocean Recharge Paradigm for ENSO. Part I: Conceptual Model.
580 Journal of the Atmospheric Sciences 54, 811-829 (1997a).
581 Jin FF. An Equatorial Ocean Recharge Paradigm for ENSO. Part II: A Stripped-Down
582 Coupled Model. Journal of the Atmospheric Sciences 54, 830-847 (1997b).
583 Jin FF, An SI. Thermocline and Zonal Advective Feedbacks Within the Equatorial Ocean
584 Recharge Oscillator Model for ENSO. Geophysical Research Letters 26, 2989–2992 (1999).
585 Jin FF, Neelin DJ. Modes of Interannual Tropical Ocean–Atmosphere Interaction—a
586 Unified View. Part I: Numerical Results. Journal of Atmospheric Sciences 50, 3477–3503 (1993).
587 Jin FF, Kim ST, Bejarano L. A coupled-stability index for ENSO. Geophysical Research
588 Letters 33, L23708 (2006).

589 Köhl A, Stammer D. Variability of the Meridional Overturning in the North Atlantic
590 from the 50-Year GECCO State Estimation. Journal of Physical Oceanography 38, 1913-1930
591 (2008).
592 Meinen CS, McPhaden MJ. Observations of Warm Water Volume Changes in the
593 Equatorial Pacific and Their Relationship to El Niño and La Niña. Journal of Climate 13, 3551-
594 3559 (2000).
595 Ray S, Swingedouw D, Mignot J, Guilyardi E. Effect of surface restoring on subsurface
596 variability in a climate model during 1949-2005. Climate Dynamics 44, 2333-2349 (2015).
597 Ren HL, Jin FF. Recharge Oscillator Mechanisms in Two Types of ENSO. Journal of
598 Climate 26, 6506-6523 (2013).
599 Santoso A, McGregor S, Jin FF, Cai W, England MH, An SI, McPhaden MJ, Guilyardi E.
600 Late-twentieth-century emergence of the El Niño propagation asymmetry and future
601 projections. Nature 504, 126–130 (2013).
602 Schopf PS, Suarez MJ. Vacillations in a Coupled Ocean-Atmosphere Model. Journal of
603 the Atmospheric Sciences 45, 549-566 (1988).
604 Singh A, Delcroix T. Eastern and Central Pacific ENSO and their relationships to the
605 recharge/discharge oscillator paradigm. Deep-Sea Research I 82 32-43 (2013).
606 Trenberth KE, Hoar TJ. The 1990-1995 El Niño-Southern Oscillation Event: Longest on
607 Record. Geophysical Research Letters 23, 57-60 (1996).
608 Wang B. Kelvin waves. In Encyclopedia of Atmospheric Sciences, Ed M Shankar,
609 Elsevier, Amsterdam, 1062-1068 (2002).
610 Wyrtki K. El Niño-The Dynamic Response of the Equatorial Pacific Oceanto
611 Atmospheric Forcing. Journal of Physical Oceanography 5, 572-584 (1975).

612 Yu Z, McCreary JP, Kessler WS, Kelly KA. Influence of equatorial dynamics on the
613 Pacific North Equatorial Countercurrent. Journal of Physical Oceanography 30, 3179-3190
614 (2000).
615 Yu JY, Mechoso CR. A Coupled Atmosphere–Ocean GCM Study of the ENSO Cycle.
616 Journal of Climate 14, 2329-2350 (2001).
617

Figure 1. Climatological temperature and ocean currents.

Multi-product average of potential temperature (°C, shading and contours in a-f) and zonal (a-c), meridional (d-f) and vertical (a-f) ocean velocities (m/s, arrows) averaged in latitude over the south off-equatorial (8-4S, a), equatorial (2S-2N, b), and north off-equatorial (4-8N, c) regions, and averaged in longitude in the western (150-160E, d), central (160-150W, e) and eastern (100-90W, f) Pacific (see the vertical green lines). The temperature contour interval is 1 °C, and the thick contour corresponds to the 20 °C isotherm.

Figure 2. Same as Figure 1, but for the difference of El Niño minus La Niña years.

The temperature contour interval is 0.25 °C, and the thick contour corresponds to the 0 °C isotherm.

Figures 3. Multi-product average of temperature tendency and heat advection during the growing phase of the heat buildup leading to El Niño events.

Anomalous zonal and vertical velocity (m/s, arrows in a), potential temperature (°C, shading in a), its time tendency (°C/year, contours in b-h) and zonal (shading in b,e,f), meridional (shading in e,g) and vertical (shading in b,e,h) heat advection (°C/year). The shading in panels c and d corresponds to the advection of anomalous heat by climatological zonal and vertical currents and the advection of climatological temperature by anomalous zonal and vertical currents, respectively (°C/year). Composite anomalies are averaged over the equatorial band (2S-2N), and shown for lag 30 months before the major El Niño events. The contour interval is 0.25 °C/year, with solid (dashed) lines depicting positive (negative) anomalies. The black (green) curve in panel a shows the climatological (anomalous) 20 °C isotherm. The dark (light) stippling denotes areas where heat advection anomalies have the same sign and magnitude larger than ±0.25 °C/year for all (all but one) the members of the ensemble.

Figure 4. Same as Figures 3a,e-h, but for the meridional transect of anomalous temperature and currents, and heat advection in the 150-160E sector.

Figure 5. Same as Figures 3a,b,e-h, but for the meridional transect of anomalous temperature and currents, and heat advection in the 160-150W sector.

Figure 6. Same as Figure 3h, but for the individual members of the ensemble.

Figure 7. Same as Figure 3g, but for the individual members of the ensemble.

Figure 8. Multi-product average of temperature tendency and heat advection during the growing phase of the recharge mode leading to El Niño events.

Anomalous zonal and vertical velocity (m/s, arrows in a), potential temperature (°C, shading in a), its time tendency (°C/year, contours in b-j) and zonal (shading in b,c,f), meridional (shading in b,g) and vertical (shading in b,c,h) heat advection (°C/year). The shading in panels d,i and e,j corresponds to the advection of anomalous heat by climatological currents and the advection of climatological temperature by anomalous currents, respectively (°C/year). Composite anomalies are averaged over the equatorial band (2S-2N), and shown for lag 21 months before the major El Niño events. The contour interval is 0.25 °C/year, with solid (dashed) lines depicting positive (negative) anomalies. The black (green) curve in panel a shows the climatological (anomalous) 20 °C isotherm. The dark (light) stippling denotes areas where heat advection anomalies have the same sign and magnitude larger than ±0.25 °C/year for all (all but one) the members of the ensemble.

Figure 9. Same as Figure 8a,c,f-h, but for the meridional transect of anomalous temperature and currents, and heat advection in the 160-150W sector.

Figure 10. Same as Figure 8c, but for the individual members of the ensemble.

Figure 11. Same as Figure 8g, but for the individual members of the ensemble.

Figure 12. Multi-product average of temperature tendency and heat advection during the growing phase of El Niño events.

Anomalous zonal and vertical velocity (m/s, arrows in a), potential temperature (°C, shading in a), its time tendency (°C/year, contours in b-h) and zonal (shading in b,e,f), meridional (shading in e,g) and vertical (shading in b,e,h) heat advection (°C/year). The shading in panels c and d corresponds to the advection of anomalous heat by climatological meridional currents and the advection of climatological temperature by anomalous meridional currents, respectively (°C/year). Composite anomalies are averaged over the equatorial band (2S-2N), and shown for lag 9 months before the major El Niño events. The contour interval is 0.25 °C/year, with solid (dashed) lines depicting positive (negative) anomalies. The black (green) curve in panel a shows the climatological (anomalous) 20 °C isotherm. The dark (light) stippling denotes areas where heat advection anomalies have the same sign and magnitude larger than ±0.25 °C/year for all (all but one) the members of the ensemble.

Figure 13. Same as Figure 12, but for the meridional transect of anomalous temperature and currents, and heat advection in the 160-150W sector.

Figure 14. Multi-product average of temperature tendency and heat advection before and after the peak of El Niño events.

Anomalous potential temperature (°C, shading in a), its time tendency (°C/year, contours in a-j) and zonal (shading in b,c,f), meridional (shading in b,g) and vertical (shading in b,c,h) heat advection (°C/year). The shading in panels d,i and e,j corresponds to the advection of anomalous heat by climatological currents and the advection of climatological temperature by anomalous currents, respectively (°C/year). Composite anomalies are averaged over the equatorial band (2S-2N) at the depth of the tilted thermocline. The contour interval is 0.50 °C/year, with solid (dashed) lines depicting positive (negative) anomalies. For clarity, the 0 °C/year contour is the only line shown in panels b-j (thick curve). The solid (dashed) horizontal green line shows the phase corresponding to the peak of EN events (LN-like conditions). The stippling denotes anomalies in which heat advection has the same sign and magnitude larger than ±0.25 °C/year for all the members of the ensemble.

Figure 15. Same as Figure 14, but along the latitudinal axis and averaged over the longitude range 160-150W.

Note that panel e shows the advection of climatological temperature by anomalous zonal and vertical currents (°C/year).

Figure 1
Click here to download Rendered Figure: Figure 1.jpg

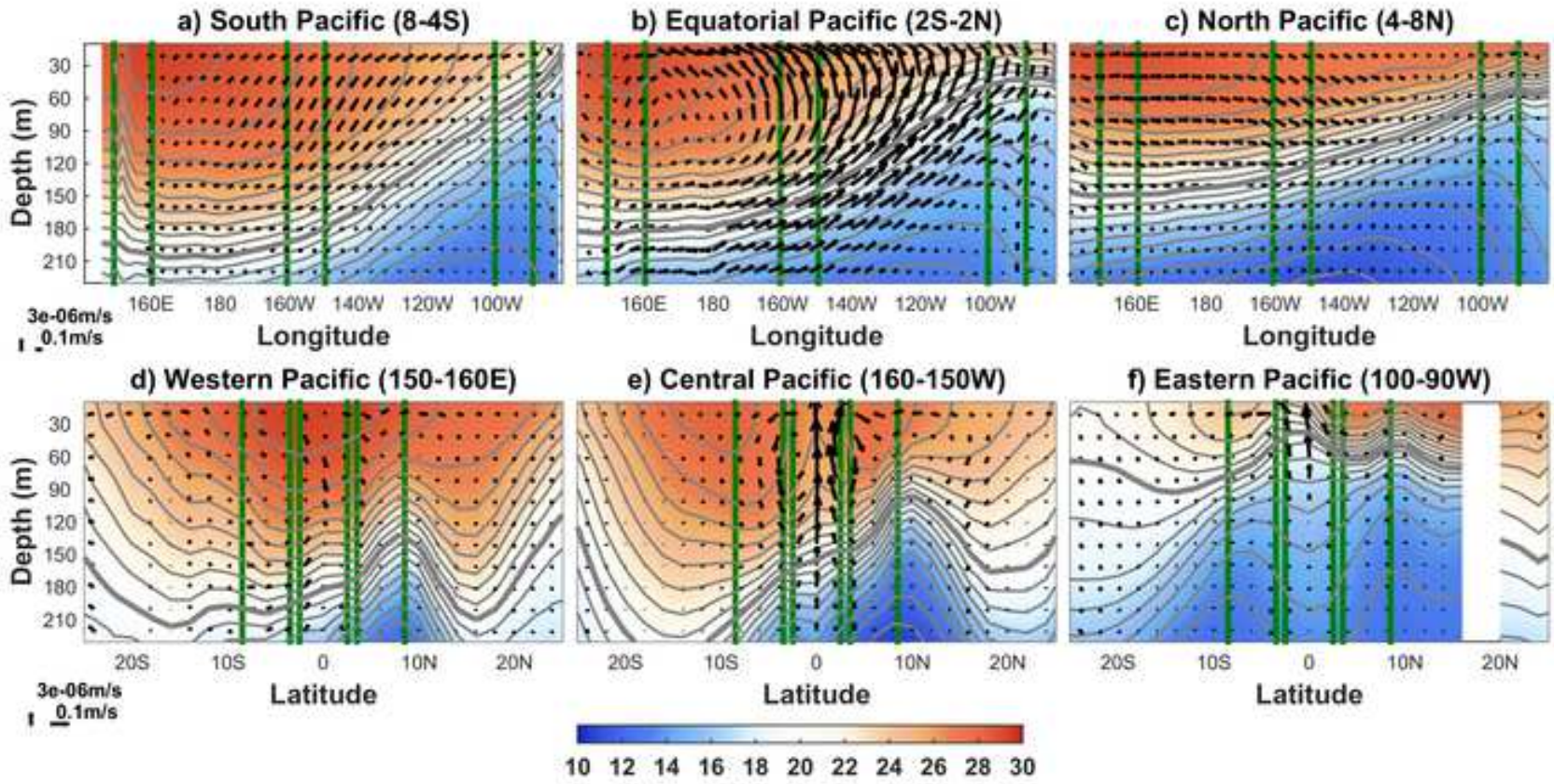

Figure 2
Click here to download Rendered Figure: Figure 2.jpg

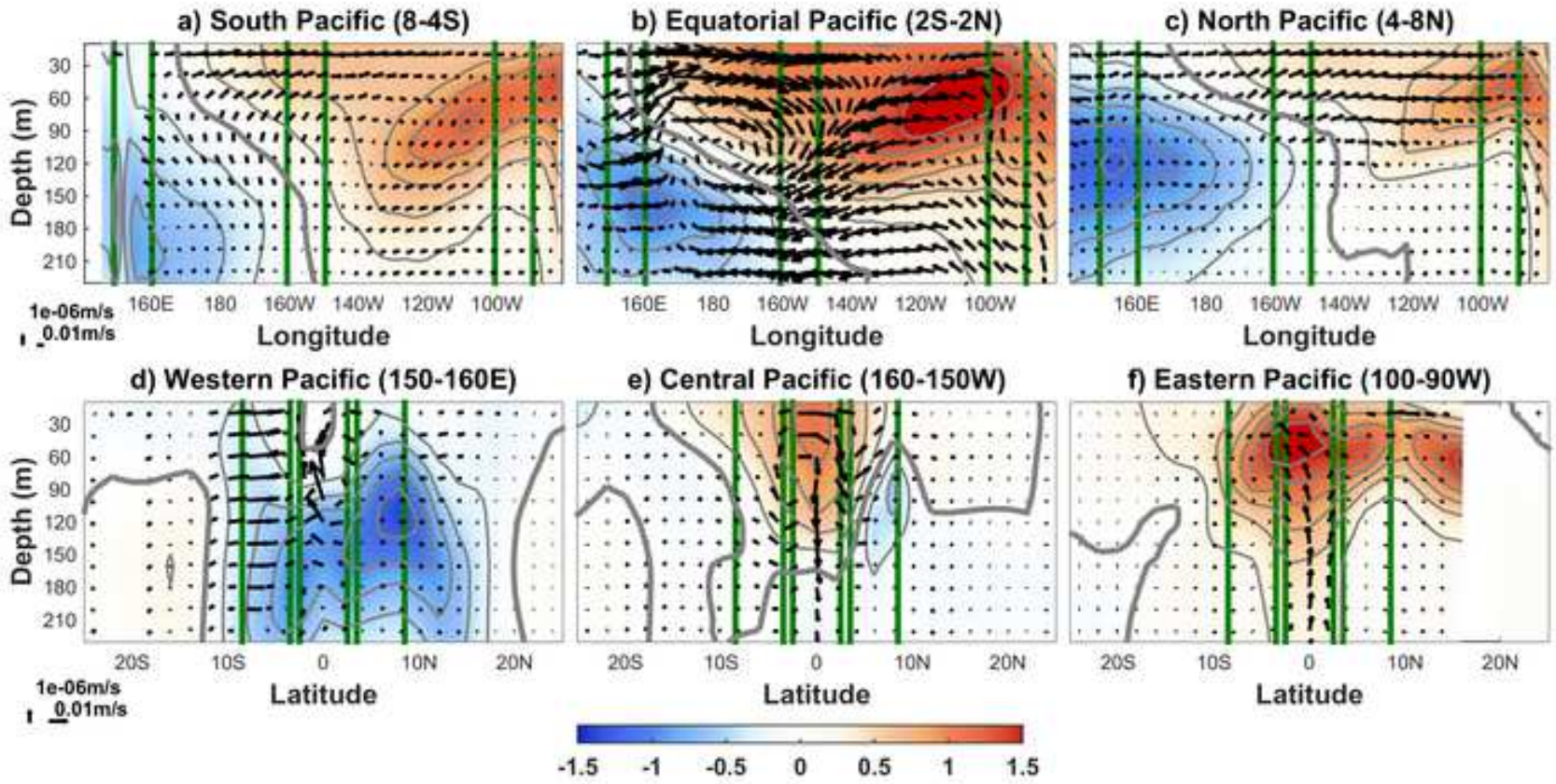

Figure 3
Click here to download Rendered Figure: Figure 3.jpg

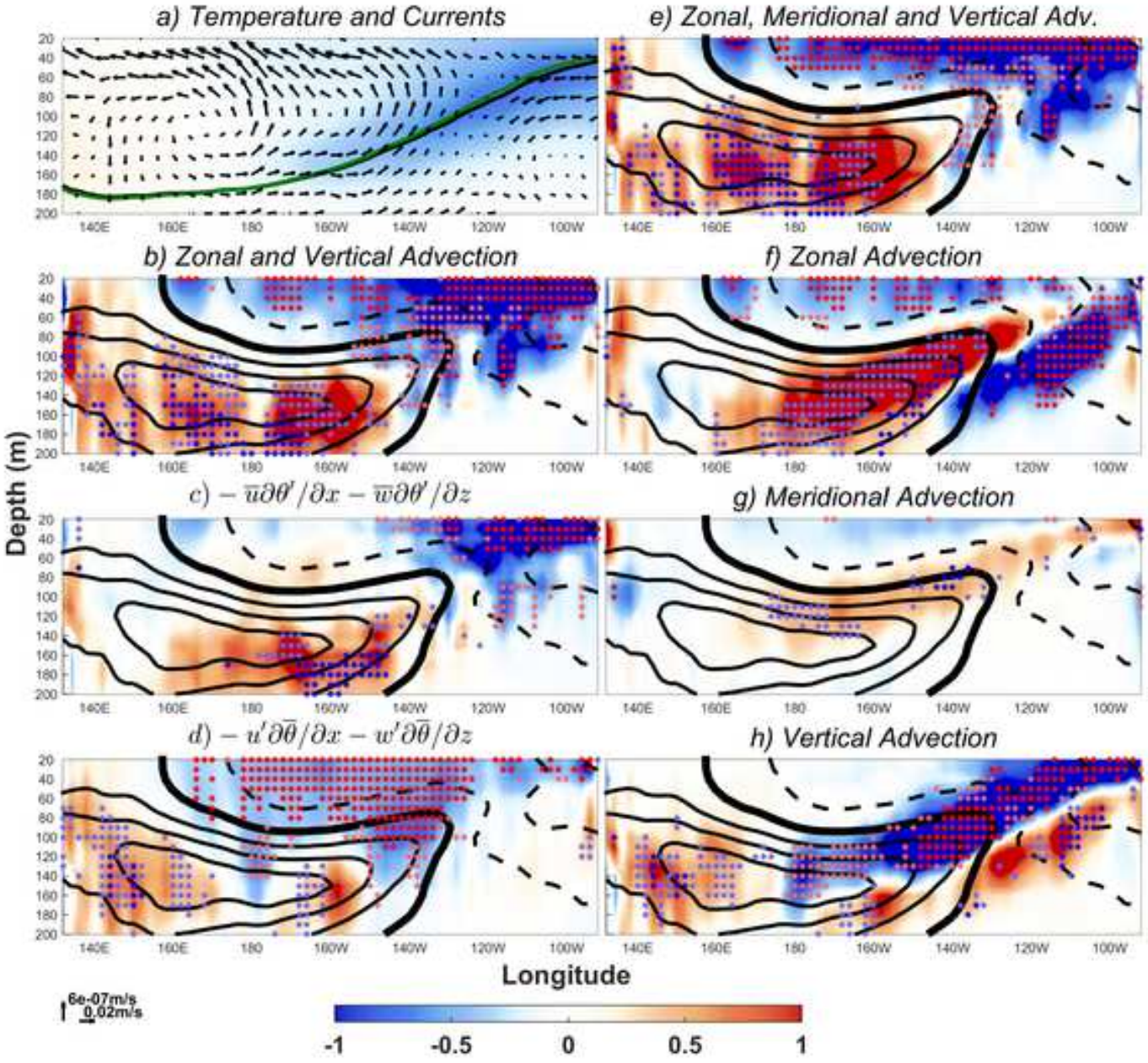

Figure 4
Click here to download Rendered Figure: Figure 4.jpg

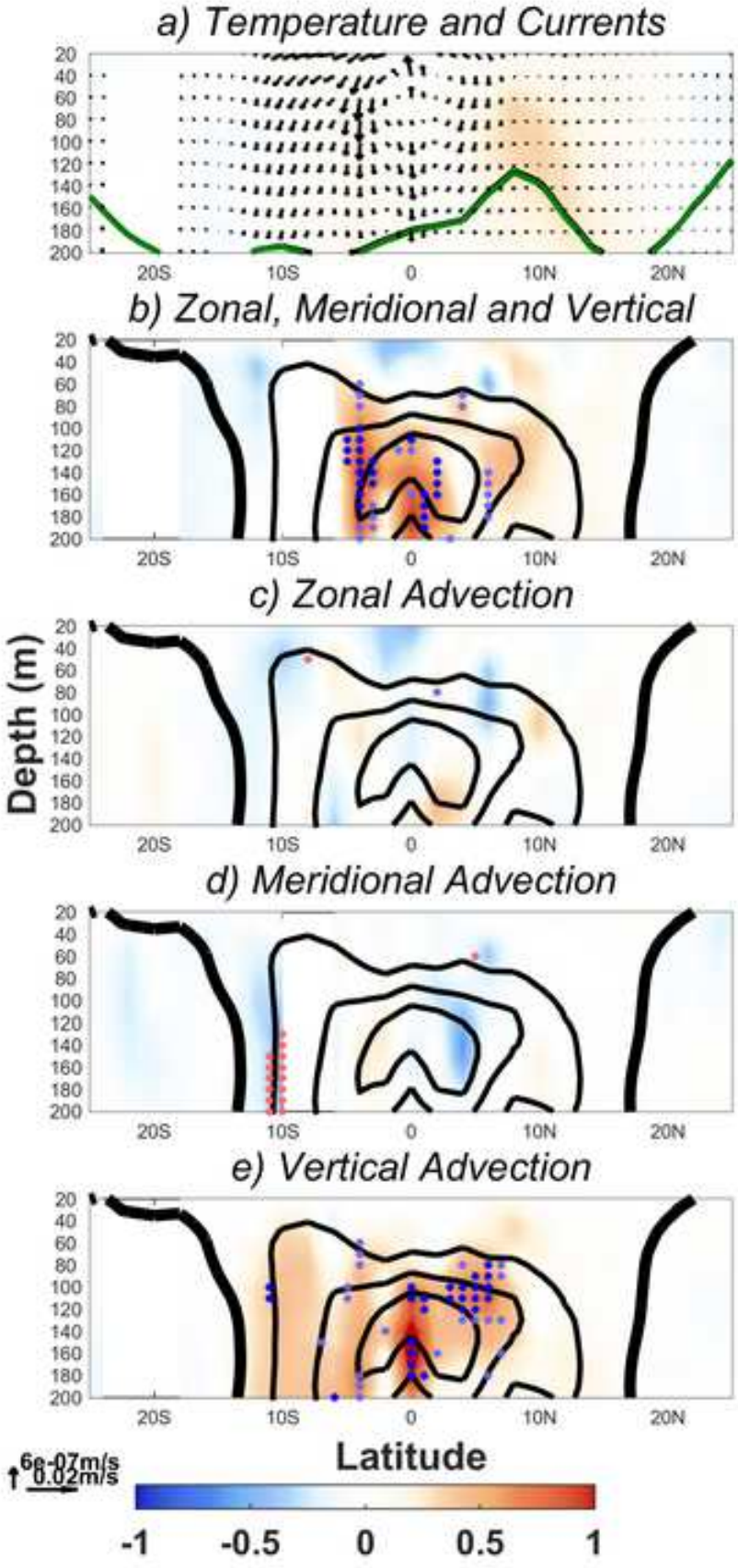

Figure 5
Click here to download Rendered Figure: Figure 5.jpg

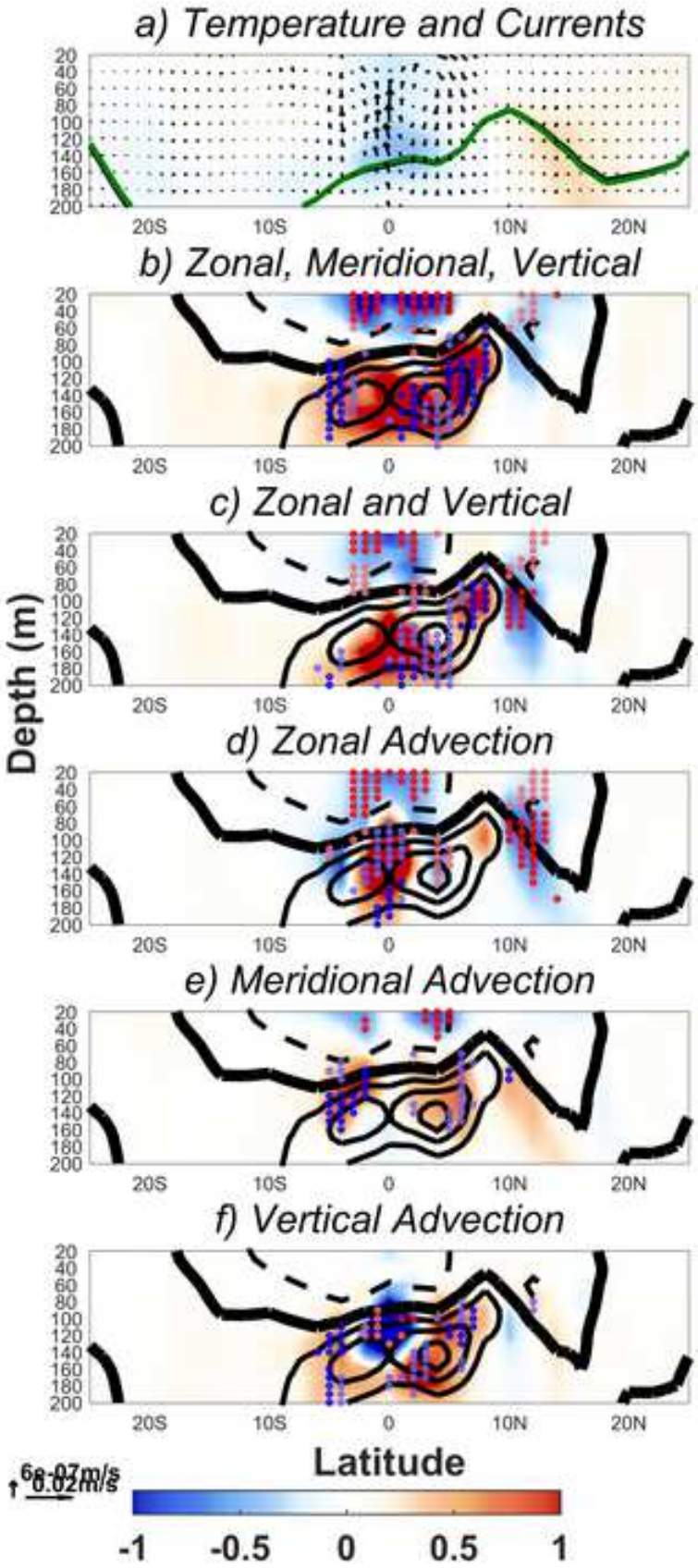

Figure 6
Click here to download Rendered Figure: Figure 6.jpg

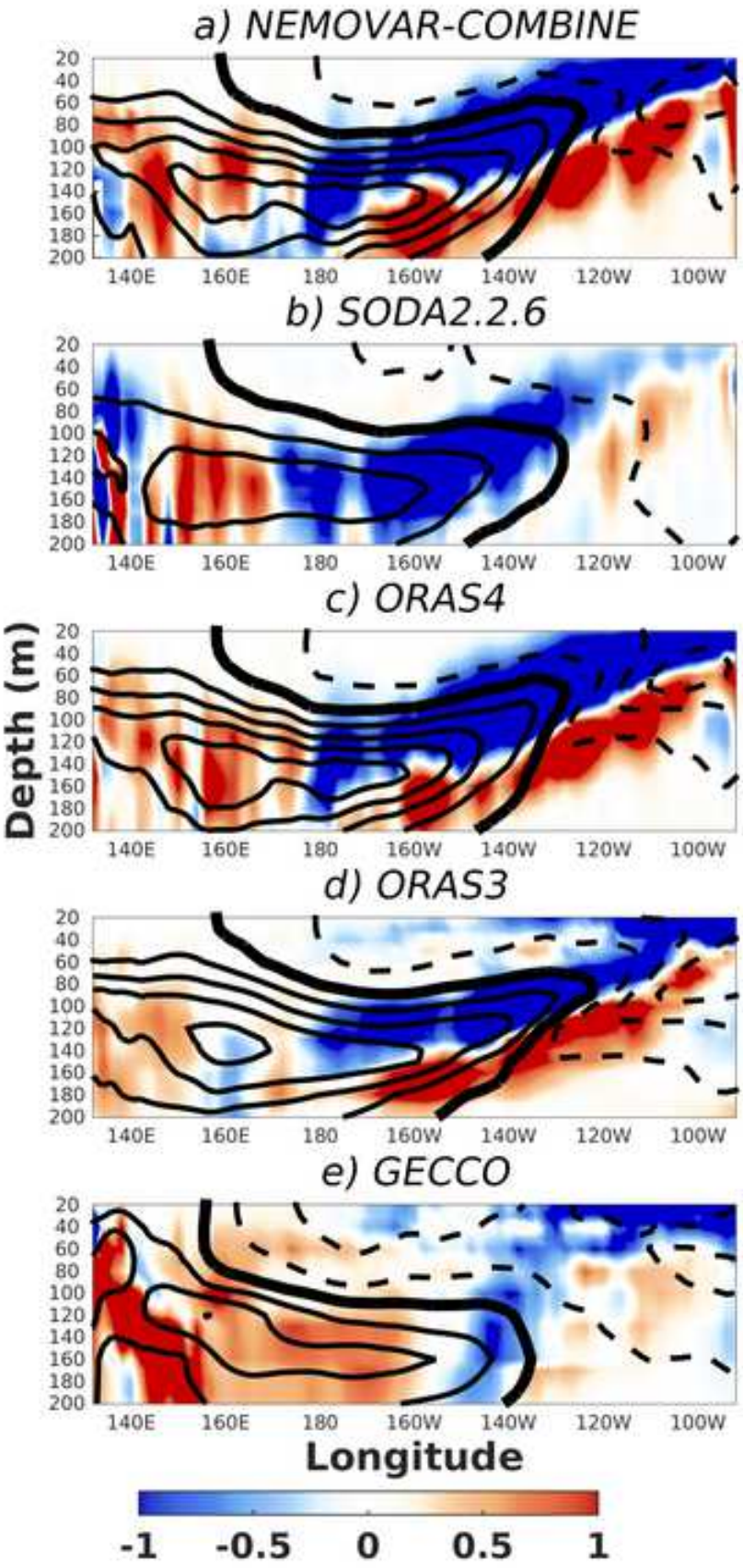

Figure 7
Click here to download Rendered Figure: Figure 7.jpg

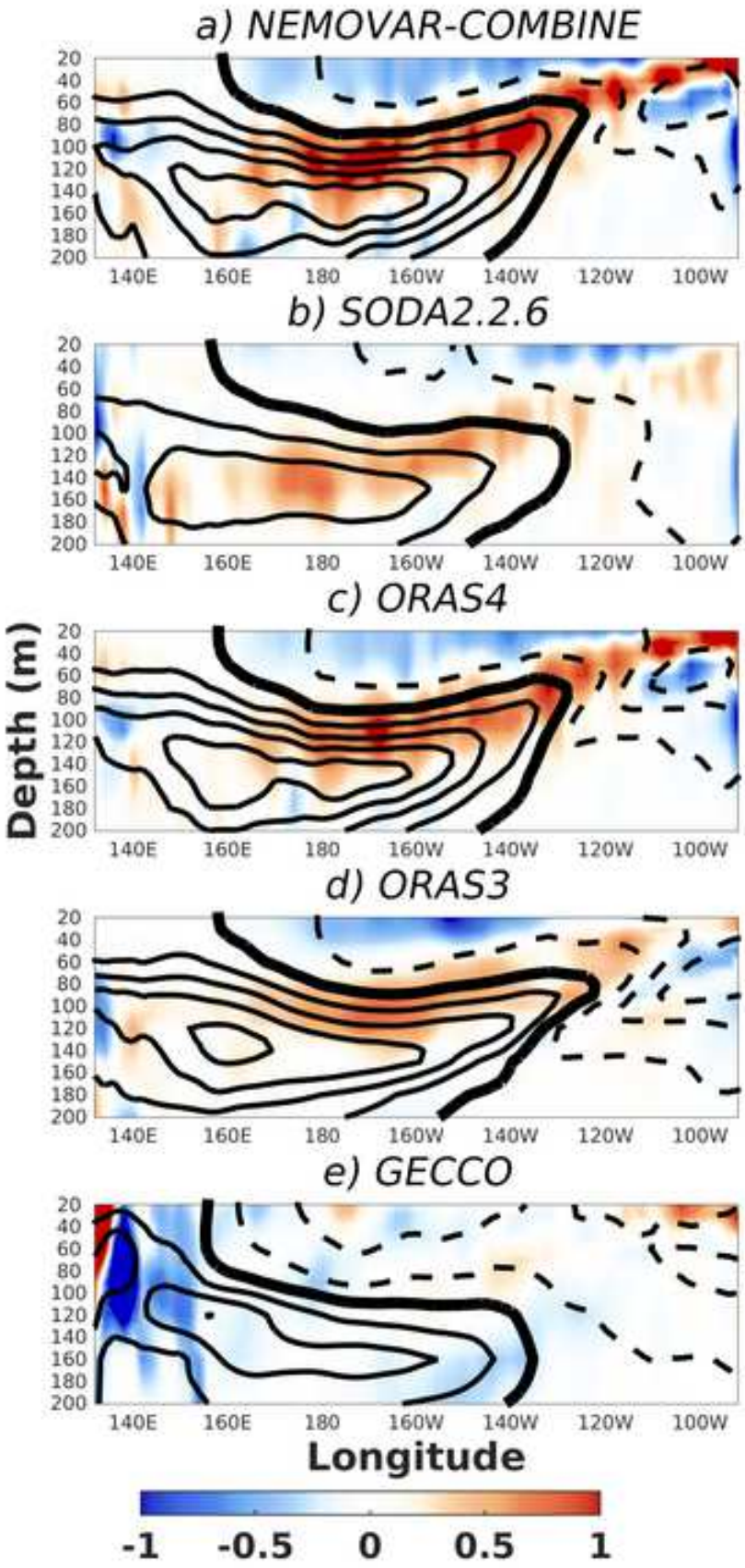

Figure 8
Click here to download Rendered Figure: Figure 8.jpg

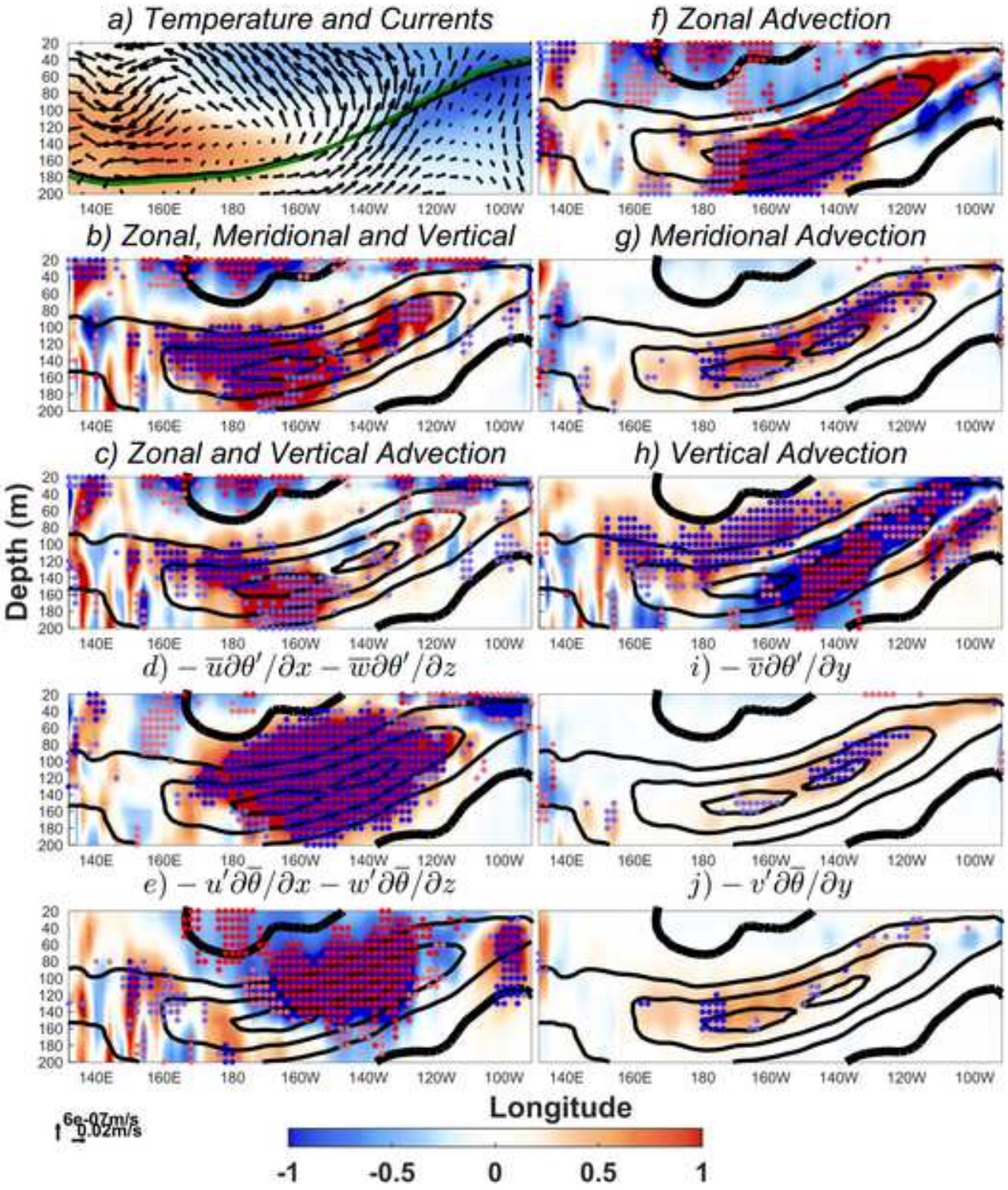

Figure 9
Click here to download Rendered Figure: Figure 9.jpg

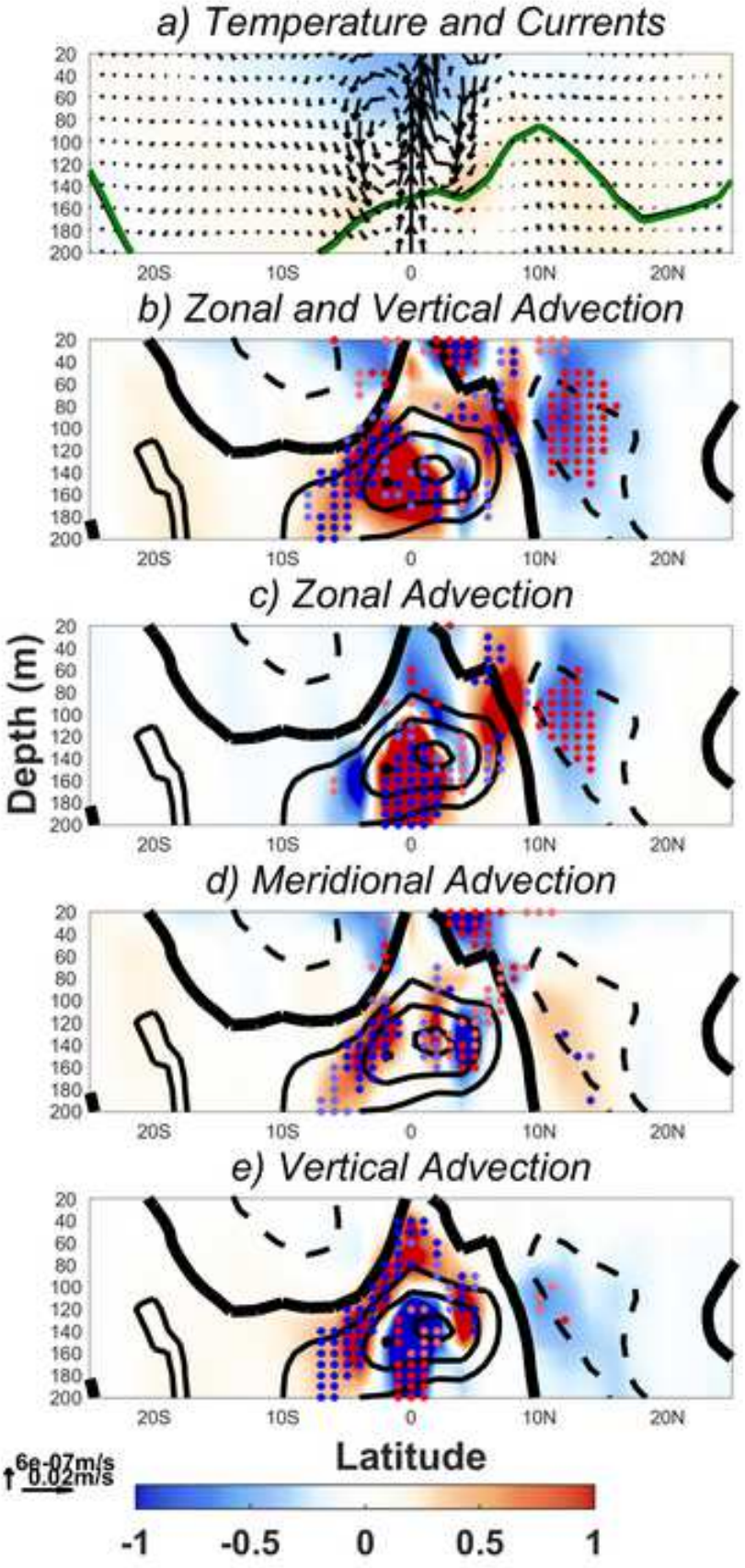

Figure 10
Click here to download Rendered Figure: Figure 10.jpg

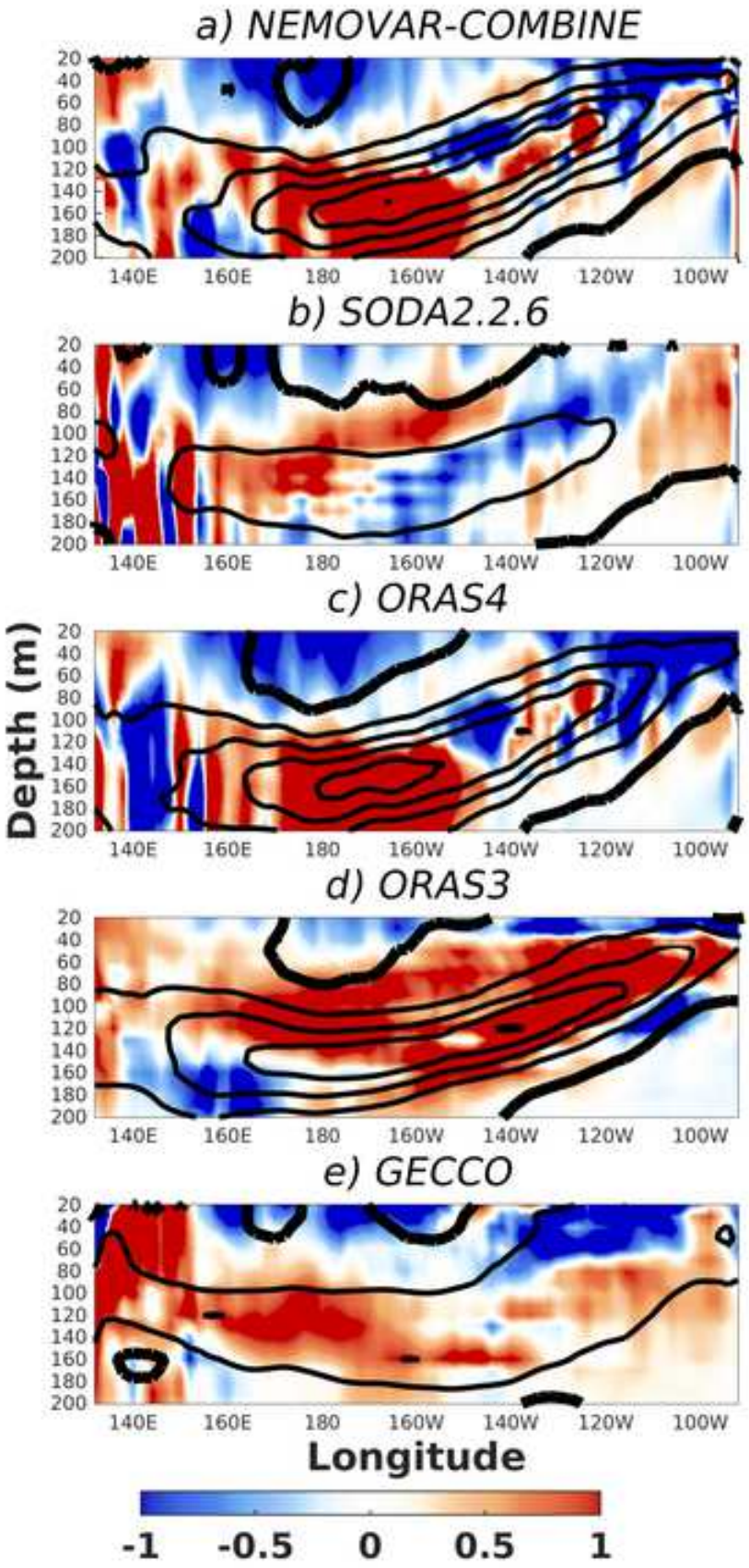

Figure 11
Click here to download Rendered Figure: Figure 11.jpg

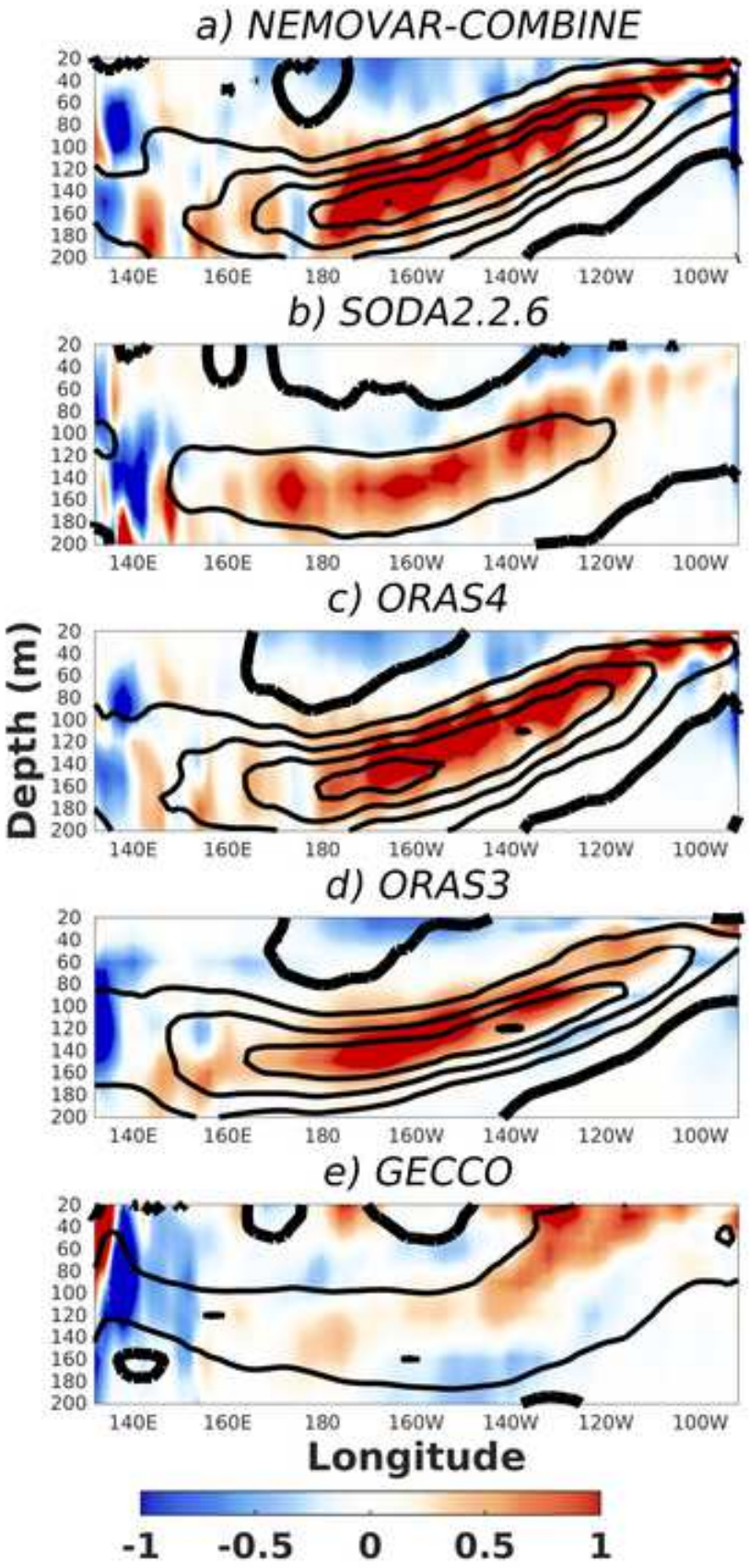

Figure 12
Click here to download Rendered Figure: Figure 12.jpg

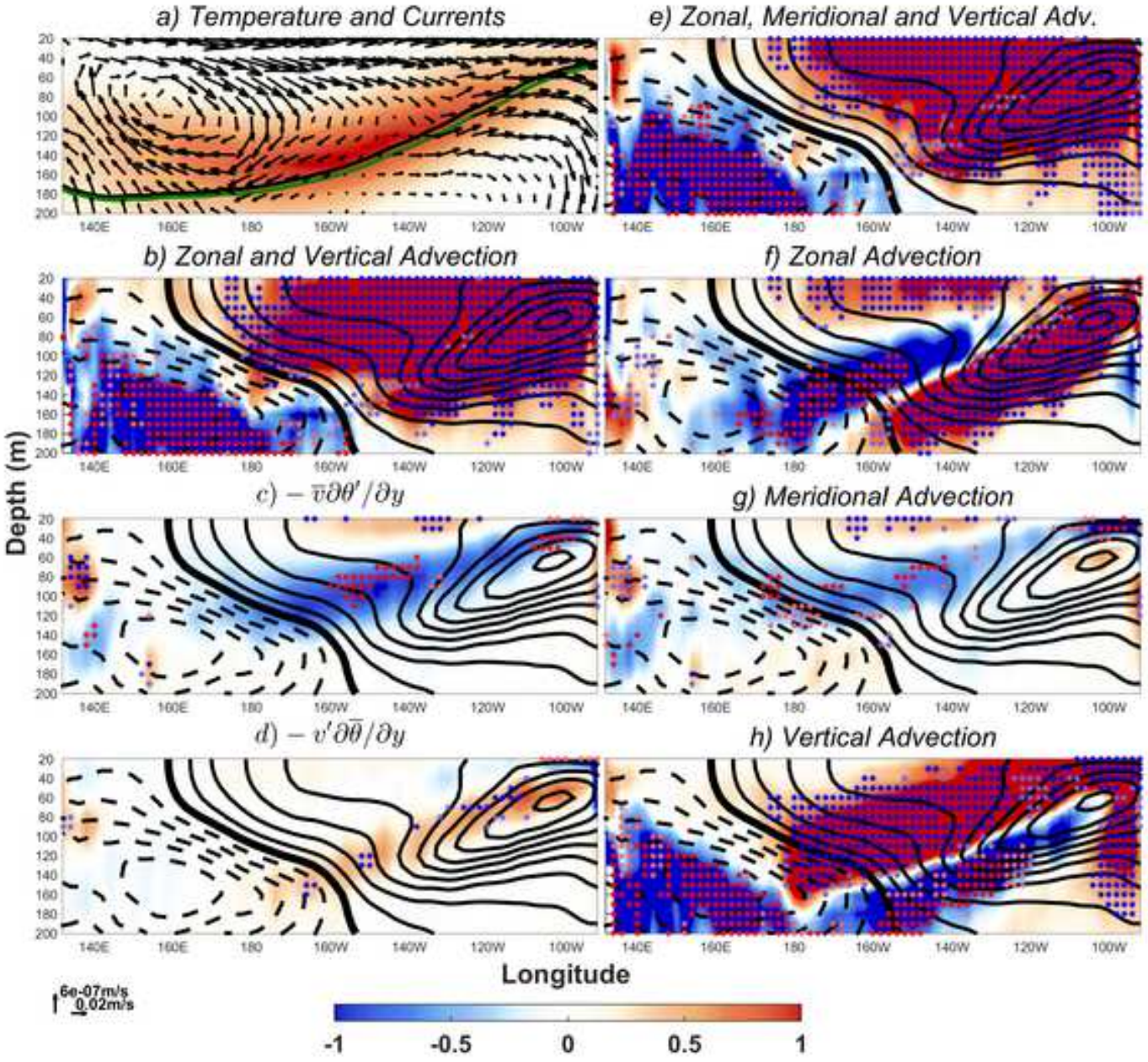

Figure 13
Click here to download Rendered Figure: Figure 13.jpg

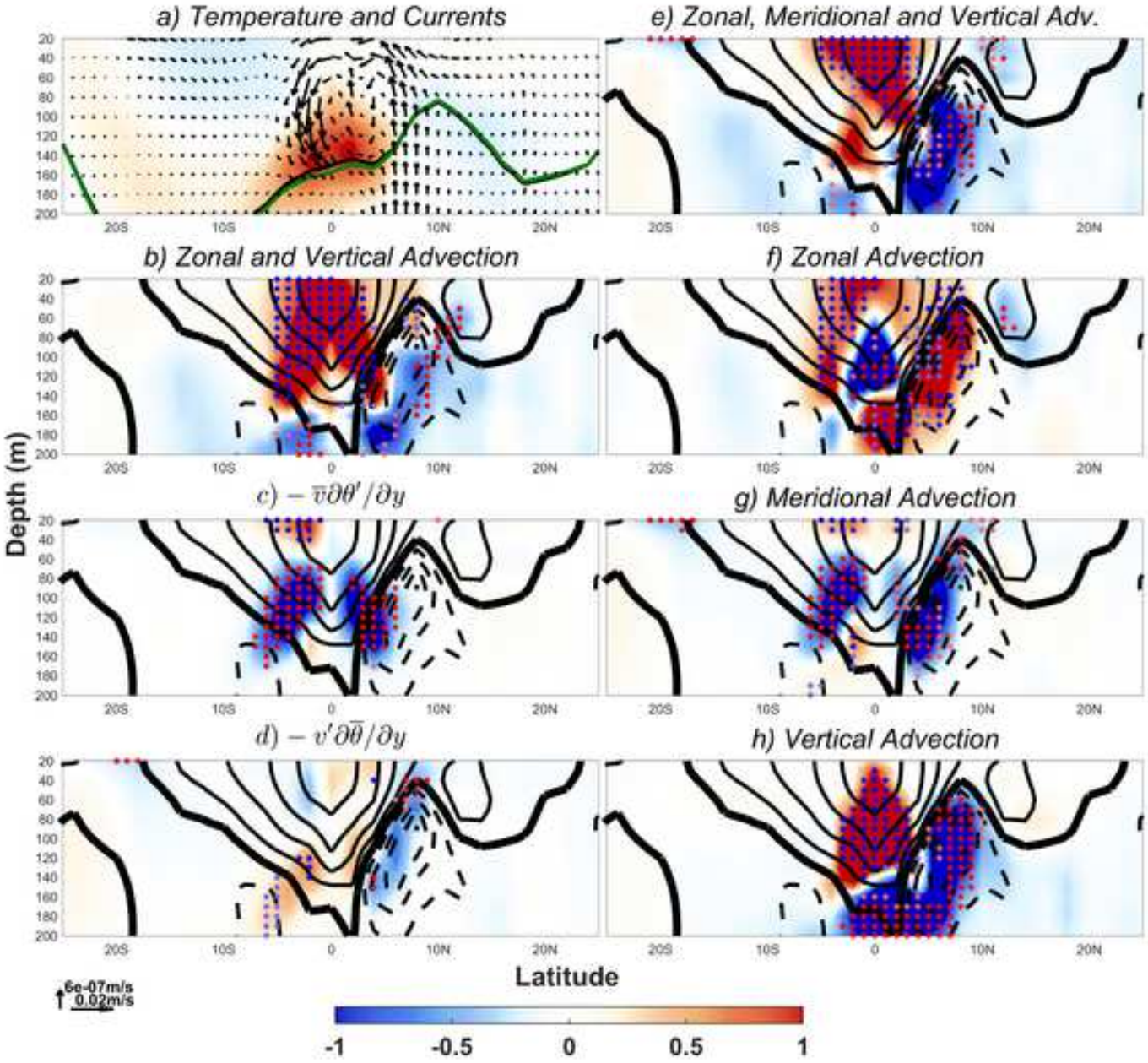

Figure 14
Click here to download Rendered Figure: Figure 14.jpg

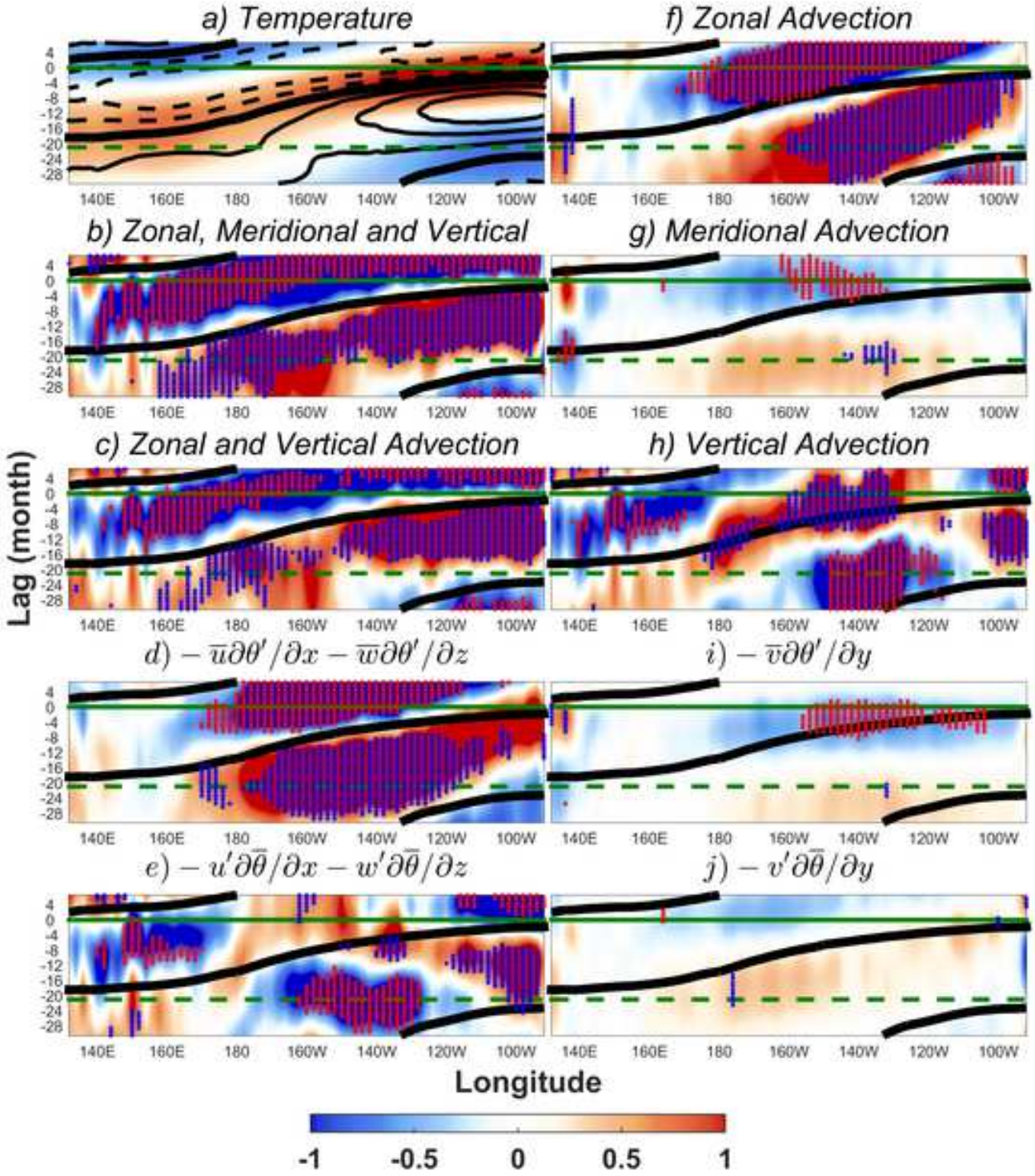

Figure 15
Click here to download Rendered Figure: Figure 15.jpg